ISBN: 978-3-95450-253-0 ISSN: 2673-5571 doi:10.18429/JACoW-HB2023-MOA1I2

FRIB FROM COMMISSIONING TO OPERATION*

P. N. Ostroumov†, K. Fukushima, A. Gonzalez, K. Hwang, T. Kanemura,
T. Maruta, A. Plastun, J. Wei, T. Zhang, Q. Zhao
Facility for Rare Isotopes Beams, Michigan State University, East Lansing, MI, USA

Abstract

The Facility for Rare Isotope Beams (FRIB) was fully commissioned in early 2022, and the operation for physics experiments started shortly thereafter. Various ion beam species have been accelerated up to 240 MeV/u and delivered to the target. During the first year of user operations, the FRIB provided 4252 beam hours with 91% availability for nuclear science. In addition, FRIB delivered about 1000 hours of various ion beam species at beam energies up to 40 MeV/u for single-event experiments. Typically, the experiments with a specific species rare isotope beam last a week or two. Each experiment requires a different primary beam species with specific energies. The primary beam power has been gradually increased from 1 kW to 10 kW over the past 1.5 years. The Accelerator Physics (AP) group develops high-level physics applications to minimize machine set-up time. Focuses include identifying beam halo sources, controlling emittances of multiple-charge-state beams, and studying the beam loss mechanisms to prepare for the ultimate 400 kW operation. This paper discusses the experience and challenges of operating a high-power CW heavy ion accelerator.

INTRODUCTION

The FRIB is a major DOE nuclear physics research facility that will provide access to 80% of all isotopes predicted to exist in nature. FRIB construction started in 2013 and finished in 2022, on cost and ahead of schedule. The beam commissioning began in 2017, first with the Front End and continued until January 2022, when the fragment separator was commissioned with a 210 MeV/u ^{36}Ar beam. During operations, installation of accelerator equipment has been taking place interrupted with short, 1-2 weeks commissioning periods. Results of each stage have been reported in multiple conference proceedings and journal papers [1-5]. The FRIB facility is based on a high energy heavy-ion CW superconducting driver linac, capable of accelerating uranium ions to 200 MeV/u and higher energies for lighter ions with 400 kW power on-target [1]. The layout of the linac is shown in Fig. 1. In this paper, we report results of the final commissioning stage, the first year of operation, and ongoing developments to support experiments with various ion beam species and the beam power ramp-up from 1 kW to 10 kW. We also discuss R&D initiatives to reach the ultimate beam power of 400 kW. To date, the primary ion beams of ^{36}Ar, ^{40}Ar, ^{48}Ca, ^{64}Zn, ^{70}Zn, ^{82}Se, ^{86}Kr, ^{124}Xe, and ^{198}Pt up to 240 MeV/u have been delivered to the target and used to produce more than 200 unstable isotopes for 12 nuclear physics experiments.

* This material is based upon work supported by the U.S. Department of Energy, Office of Science, Office of Nuclear Physics and used resources of the FRIB, which is a DOE Office of Science User Facility, operated by Michigan State University, under Award Number DE-SC0000661.
† Ostroumov@frib.msu.edu

FRONT END

The linac Front End (FE) includes two Electron Cyclotron Resonance (ECR) ion sources, a Low Energy Beam Transport (LEBT) section that selects desired ion species, a Radiofrequency Quadrupole (RFQ), and a Medium Energy Beam Transport (MEBT) section. Proper tuning of the FE is critical to provide low-emittance and low-halo beams at the entrance of the SC linac. The main strategies for the beam tuning in the FE have been discussed in previous publications (see [3] and references therein).

Initial ion beams are produced by a room temperature Electron Cyclotron Resonance (ECR) ion source, ARTEMIS, for the linac commissioning and initial operation [6]. At the beginning of this year, a new superconducting High Power ECR (HP-ECR) was commissioned [7]. The new HP-ECR significantly increased the flexibility of the FRIB to prepare and provide various ion species for experiments. In addition, the new HP-ECR and following beam transport produce a higher quality beam. To reduce the beam halo at the entrance to the SC linac, we started using two round collimators in the LEBT positioned for proper collimation in the phase space. These collimators remove 5-10% of the total beam intensity and result in a more compact beam phase-space. The beam profile measurements in the MEBT shown in Fig. 2 illustrate the effectiveness of the collimation.

Machine Learning Application in Front End

The unknown distribution of mechanical misalignments in the FE results in simulated beam trajectory predictions being insufficiently accurate for on-axis RFQ injection tuning. A “black-box” local optimization using the Nelder-Mead method and data from BPMs and post-RFQ Faraday Cup (FC) measurements, has been utilized until recently for beam centering and current maximization. However, local optimum solutions obtained were often not satisfactory. Therefore, we developed a Machine Learning (ML) tool based on Bayesian optimization to more efficiently explore the global decision domain utilizing all the collected data during the optimization procedure. We tailored the improved optimization algorithm to minimize corrector magnet ramping time and magnet polarity crossings which is the major time-consuming factor. We suppressed polarity changes by favoring the decision candidates with the same polarity at the present magnet set values in the acquisition function used for the decision candidate search. The polarity favouring is carefully structured so as not to limit the capability of searching for the optimum tune. The objective

ISBN: 978-3-95450-253-0 ISSN: 2673-5571 doi:10.18429/JACoW-HB2023-MOA1I2

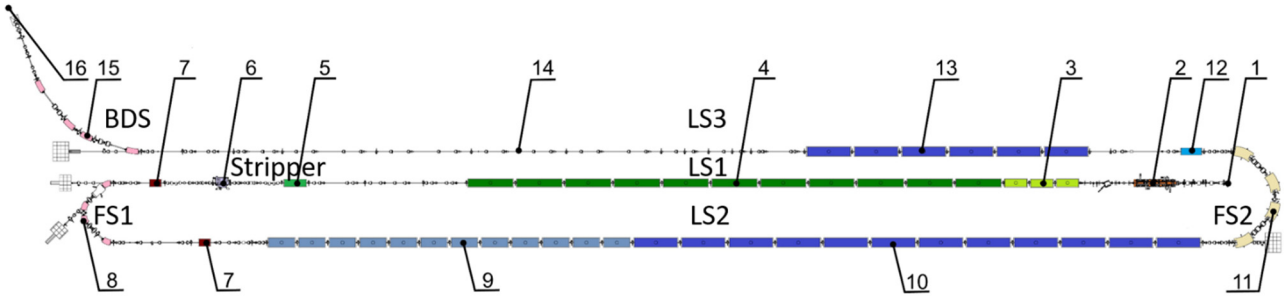

Figure 1: Layout (top view) of the FRIB accelerator in the tunnel (the above-grade portion of the Front End is not shown). 1 – ten-meter vertical drop from ion sources (above ground); 2 – 0.5 MeV/u RFQ; 3 – three β = 0.041 QWR cryomodules; 4 – eleven β = 0.085 QWR cryomodules; 5 – β = 0.085 bunching cryomodule; 6 – Lithium and carbon stripper modules; 7 – multi-gap buncher; 8 – room temperature folding segment; 9 – twelve β = 0.29 HWR cryomodules; 10 – twelve β = 0.54 HWR cryomodules; 11 – superconducting folding segment; 12 – β = 0.53 bunching cryomodule; 13 – six β = 0.53 HWR cryomodules; 14 – beam transport to the target; 15 – beam delivery system (BDS); 16 – fragmentation target. Linac Segment 1 (LS1): 3-5; Folding Segment 1 (FS1): 7-8; Linac Segment 2 (LS2): 9-10; Folding Segment 2 (FS2): 11; Linac Segment 3 (LS2): 12-14; Beam Delivery System (BDS): 15.

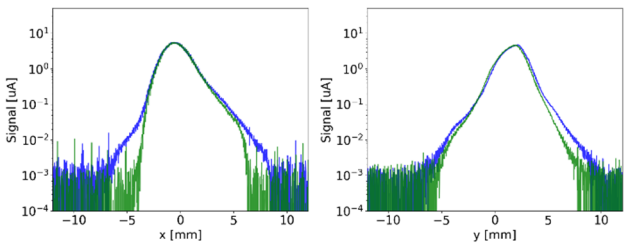

Figure 2: Horizontal (left) and vertical (right) wire-scanner measured $^{124}Xe^{26+}$ beam charge profiles in the MEBT with and without collimators inserted.

is also carefully tailored to minimize beam emittance. Our experience shows that the minimization of transverse beam loss (measured using the ratio of two BCMs) within the RFQ is correlated to smaller beam emittance. This algorithm was successfully demonstrated and is now used routinely for FE tuning.

STRIPPING AND CHARGE SELECTION

To overcome the technical limitations associated with stripping high-intensity heavy ion beams with thin foils, FRIB developed and commissioned a liquid lithium stripper [8]. The charge stripper is based on molten liquid lithium film with a ~10-20 μm thickness, flowing at ~60 m/s in the vacuum environment. A rotating carbon foil disk is also installed next to the lithium stripper and has been successfully used for stripping ions lighter than xenon with beam intensities up to 10 kW on-target. The ion beam must be focused into a small spot < 0.5 mm rms radius on the lithium film to avoid the film's non-uniformity negatively impacting the beam energy spread. Liquid lithium film thickness measured with the ion beam is shown in Fig. 3. The analysis of the film thickness variations indicates that the most uniform area is near $(x, y) = (-0.7\ \text{mm},\ 1.0\ \text{mm})$ and corresponds to 1.0 mg/cm^2.

Unfortunately, except for Argon, this thickness cannot produce an equilibrium charge distribution for desired ion species. Ongoing R&D work seeks to double the lithium film thickness [8]. During the operation, sudden changes in lithium film thickness results in beam energy fluctuations and effective emittance growth. To mitigate such beam energy fluctuations, we are developing a feedback system to adjust the phases of the 2-3 cavities upstream of the stripper. A feedback system will stabilize the beam energy and maintain the constant arrival time of the bunches to the rebuncher (see 7 in Fig. 1). So far, the digital feedback system has a relatively long response time of ~200 ms. Options for reducing the response time are being pursued.

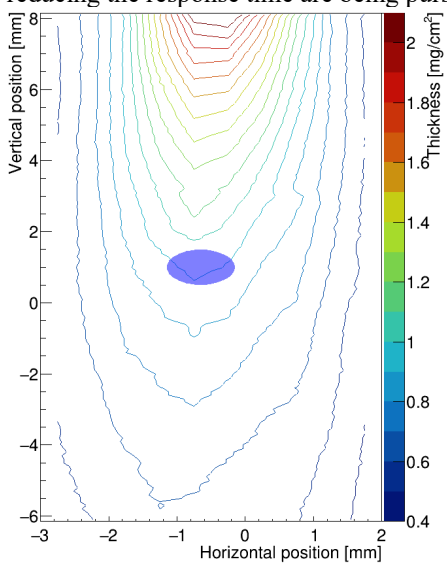

Figure 3: Liquid lithium film thickness measured with an Xe beam.

Figure 4 demonstrates the effect of the feedback system on the beam energy fluctuation after the stripper. Emittance growth and halo formation after the stripper mainly contribute to possible beam losses in LS2 (see Fig. 1). Beam losses in LS2 must be maintained at an extremely low level to avoid the unstable operation of superconducting cavities due to field emission and/or multipacting. The energy spread increase after the stripper may induce beam halo in the longitudinal phase space that may not fit into the acceptance of LS2. The temperature probes installed on the

ISBN: 978-3-95450-253-0 ISSN: 2673-5571 doi:10.18429/JACoW-HB2023-MOA1I2

beam pipes inside the LS2 cryomodules were calibrated by intentional loss of 100 mW of beam power. With the beam power on the target at a 5 kW level, beam losses in LS2 are below 50 mW. To maintain such low and acceptable beam losses in LS2 as beam power ramps up, we will increase the longitudinal acceptance by linearizing the buncher voltage over an extended phase range by using RF harmonic. Figure 5 shows the LS2 acceptance with and without harmonic cavities. The primary benefit of this increase in acceptance will occur in operation with multiple-charge-state beams.

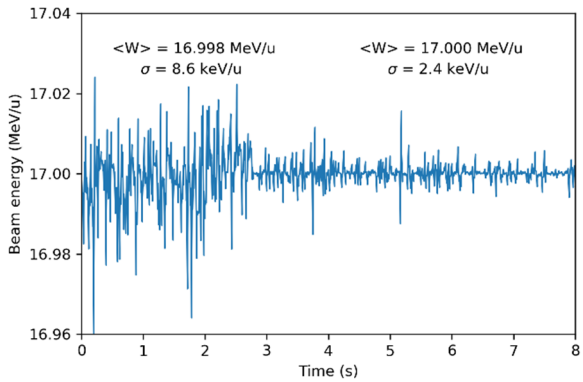

Figure 4: Measured beam energy after the liquid lithium stripper as a function of time. Note the significant reduction of the energy fluctuations when the active feedback system is on at 2.8 second.

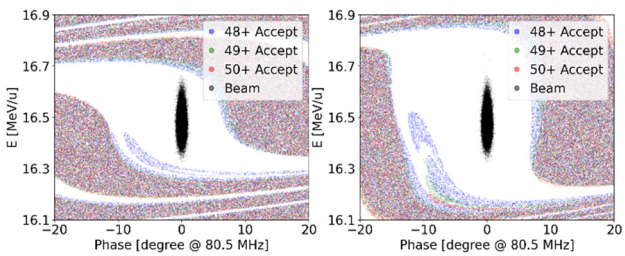

Figure 5: Simulated longitudinal phase-space acceptance of the linac section downstream of the stripper for three charge states of ^{124}Xe without (left) and with (right) the second-harmonic cavity. One million particles were tracked from the LEBT through the lithium stripper and shown with black dots.

The adjustable Charge Selector Slits (CSS) in the high-dispersion point after the 45° bending magnet in FS1 intercept the unwanted charge states of ion beam. Scraping energetic heavy ions here is a technically challenging problem due to the extremely high beam power density. The multi-charge-state acceleration after the stripper substantially reduces the deposited power of unwanted charge states. Table 1 lists simulated stripping efficiencies, η_{str}, for 1q-5q (q is the "charge state") heavy ion beams stripped with a 1.0 mg/cm^2-thick lithium film. The power depositions on the charge selector slits are listed for 100 kW beams on-target. The critical parameter defining the limits of the beam absorber is that the power deposited on a single spot should be lower than 2 kW for any beam on the list. The power limit at the CSS was calculated for Gaussian distribution with typical beam size at this location. Note that the stripping efficiency of the lithium film can be increased for all multi-q beams by thickening the film [8].

Table 1: Simulated beam power losses on the CSS for 100 kW ion beams on-target. q_{ECR},is the ion charge state after the ECR selected for the acceleration, q_{str} is the number of charge states for simultaneous acceleration after the stripper, η_{str} is the stripping efficiency.

Ion	q_{ECR}	I_{ECR}, pμA	q_{str}	η_{str}	CSS Power, W
^{36}Ar	10	15.4	1	89%	852
^{48}Ca	10	12.8	2	96%	344
^{58}Ni	16	10.0	2	95%	405
^{64}Ni	16	10.0	2	95%	446
^{64}Zn	19	9.1	2	96%	328
^{70}Zn	19	9.1	2	96%	358
^{70}Ge	19	8.9	2	92%	698
^{82}Se	14	8.8	2	90%	1010
^{78}Kr	17	8.1	2	92%	707
^{86}Kr	17	8.1	2	92%	780
^{92}Mo	19	9.4	2	69%	3740
^{124}Xe	26	6.6	3	77%	2160
^{144}Sm	26	5.6	3	80%	1860
^{198}Pt	29	5.6	3	67%	4230
^{208}Pb	32	5.8	3	62%	5320
^{209}Bi	32	5.8	3	62%	5320
^{238}U	33	4.2	5	80%	2330

HIGH-LEVEL APPLICATIONS

At FRIB, EPICS [9] is utilized to implement the online control system solution for the entire accelerator system. EPICS is interfaced to Python to allow modern dynamic programming in building high-level physics control software. On the physics high-level controls side, a software framework known as "PHANTASY", based on Python, has been designed and developed to support application development [10]. The primary mission of "PHANTASY" is to establish a middle layer for device communication from the physicist's perspective. Instead of requiring individuals to memorize process variable (PV) strings, it adopts an object-oriented approach to device control, allowing for direct input of measurement data in the physics domain for modelling purposes or for engineering uses in hardware control. Among the developed applications, the "Settings Manager" is one of the apps most used in FRIB operations [11]. It smooths management of system parameters for beam delivery between the Operators and Accelerator Physicists. This application bridges information gaps by consolidating data from various sources into one app, presenting and using data in a unified manner.

The software includes High-Level Applications (HLA) with embedded physics models. For example, the trajectory correction app employs FLAME, a fast-running linear optics-based model to calculate the orbit response matrix,

ISBN: 978-3-95450-253-0 ISSN: 2673-5571 doi:10.18429/JACoW-HB2023-MOA1I2

and within a few minutes, correct the beam centroid trajectory to on-axis over the entire linac. Similarly, the SRF cavity tuning app rapidly sets the appropriate rf cavity phases and amplitudes for the required beam energy. This app calculates the required cavity settings for different velocity profiles by integrating physics models and making hardware adjustments almost instantaneously. Continuous improvements in these applications and over 30 other HLAs support rapid development and optimization of the linac settings for any ion species. Machine operating points are also systematically archived.

INSTANT PHASE SETTING AND ENVELOPE MAPPING

Instant Phase Setting (IPS) app [12] is routinely used for phase and amplitude setting in all RF cavities in the linac. This method tremendously saves the development of the new velocity profile for the acceleration of new ion species, frequently required in FRIB to support the production of specific rare isotopes for science. We have faced calibration errors with unknown sources in the RF cavities since the RF system was not designed to maintain the phase references for a year or longer. Therefore, after completion of the calibration procedure and before a production run, we measure the phase shift between the neighbouring RF cavities over the entire linac without a beam. This data allows us to identify and correct phasing errors quickly if they occur when operating points are brought back.

Longitudinal Envelope Mapping

By selecting the phases of the MEBT bunchers, the beam center can be positioned on the matched longitudinal phase-space ellipse boundary at the LS1 entrance [12]. The envelope mapping procedure includes moving the bunch center around the phase space ellipse boundary and measuring beam phases with BPMs along the linac. The envelope of these trajectories describes the rms envelope if the initial phase space area in the MEBT is equal to the rms emittance. This method does not provide the correct mapping in the post-stripper part of the linac, due to the longitudinal emittance growth in the stripper. However, if the emittance growth is not significant, the envelope mapping provides a good understanding of the matching and stability of the beam motion. An example of the envelope mapping for a single charge state ^{48}Ca beam in the entire linac from LS1 to target is illustrated in Fig. 6.

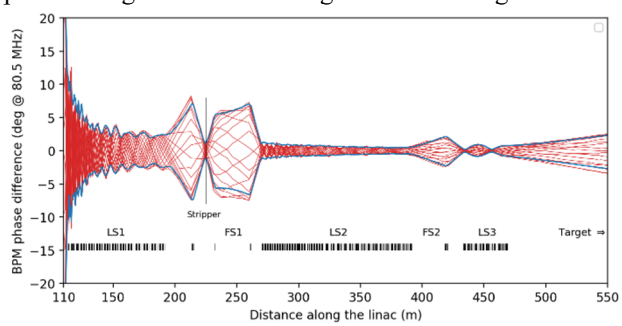

Figure 6: ^{48}Ca bunch phase longitudinal envelope mapping results in the entire linac. The IPS simulation of the phase envelope is shown in blue.

Transverse Envelope Mapping

A similar envelope mapping procedure to the longitudinal case can be applied to the transverse motion. The beam is positioned on the phase space ellipse by correctors in the MEBT and delivered to the linac. An example of transverse envelope mapping is presented in Fig. 7 for a ^{48}Ca beam in the pre-stripper (LS1) section of the linac. The envelope mapping obtained is consistent with FLAME simulations [13]. Transverse envelope mapping is a flexible tool to evaluate the quality of the beam matching. This tool is frequently used to verify beam focusing up to the target [4].

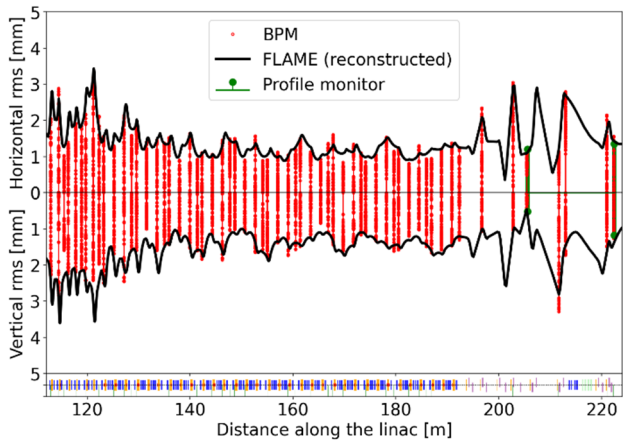

Figure 7: Transverse envelope mapping of a ^{48}Ca beam, pre-stripper linac. The black curve is the rms envelope simulated by FLAME.

TUNING OF MULTIPLE-CHARGE-STATE ION BEAMS

The linac is designed to accelerate multiple-charge-state beams after the stripper to ultimately achieve 400 kW beam power on the target. Additionally, multiple-charge-state acceleration dramatically reduces the power of unwanted charge states collimated in the CSS. The tuning of the 3q beams, such as ^{124}Xe and ^{198}Pt, has been described in previous publication [5]. The presence of the central charge state facilitates such tuning. We have also developed a dual charge state (2q) tuning procedure, which is more complicated due to the absence of the central charge state. The most challenging 2q beam is ^{48}Ca$^{19+,20+}$ due to the low charge states of 19+ and 20+ resulting in relatively large charge spread, $\Delta q/q$=5%. Phasing of cavities in LS2 and LS3 has been performed with the most intense charge state 20+ using the IPS application. At the entrance of LS2, the bunch center of each beam in the phase space is nearly identical thanks to the focusing provided by the rebuncher. For simultaneous acceleration of both charge states, the phasing of LS2 and LS3 has been shifted for 3°, so that the longitudinal motion of each charge state takes place on opposite sides in the phase space with respect to the new center. Envelope mapping performed for each charge state separately confirm (see

ISBN: 978-3-95450-253-0 ISSN: 2673-5571 doi:10.18429/JACoW-HB2023-MOA1I2

Fig. 8) the validity of this approach. Performance is improved since the stability area is better utilized. Tuning of the achromatic bends for 2q transport is carried out in two stages. First, we align the beam trajectory to the centers of quadrupoles inside the bend using the excitation currents of the dipoles and their trim coils. During this step, we align the beam centroid by changing a quadrupole's strength and minimizing variations of BPM position readings downstream of the quadrupole. If the reference charge state is not an integer, for example, 19.5+ for 2q acceleration of $^{48}Ca^{19+}$ and $^{48}Ca^{20+}$, then the magnet settings are scaled from either of the charge states to the reference one, i.e. from 20+ to 19.5+. In the second stage, we merge the beam charge states downstream of the bend. Figure 9 presents the beam tuning steps to minimize the difference between the charge states' horizontal positions and bring both onto the beamline axis. Step 1 is the initial difference and mean of the charge states' position. Step 2 is with zero sextupoles' currents. All quadrupoles' strength in the bend are adjusted in steps 3-5. In step 5, we merged the charge state, but the horizontal position is at -3.4 mm. In steps 5-7, sextupole currents are adjusted to zero the centroid (on-axis). In step 8, final adjustments of the quadrupoles are made. Optimized settings of the quadrupoles and sextupoles in the achromatic bend found experimentally under this procedure and with FLAME optimization are consistent within several percent. The residual deviation is likely due to the fringe field effects (FLAME uses a hard-edge equivalent model). The $^{64}Zn^{29+,30+}$ 2q beam was tuned most carefully in the entire linac since it has been employed for extended production runs. The measured beam centroids along the linac are shown in Fig. 10. The beam centroid correction in the linac is alternated with the transverse phase space matching at several critical sections, as described in [5]. A similar tuning procedure in the transverse phase space will be applied for additional 2q beams. Beam focusing on the target of the multi-q beams in the BDS has been described in recent publication [5]. The segmented water-cooled copper collimator located 1.5 m upstream of the target has been extremely useful in positioning the beam on-target. Four collimator segments intercept a fraction of the nearly axisymmetric beam, increasing the temperature from deposited energy. Equalizing the ΔT in each collimator segment allows centering of the beam on the target.

BEAM PROPERTIES

Primary mechanisms for beam emittance growth are interaction with the stripper material and nonlinearities of the focusing solenoids and quadrupoles. In the case of the multiple-charge-state beam, each charge state has a mismatch factor that produces effective emittance growth. Typically, we observe a factor of 2 rms emittance growth from the LEBT to the BDS for single-charge-state beams, and a factor of 3 growth for multiple-charge-state beams. The emittance growth does not result in measurable beam losses -- except in the BDS area, where we can see signals from the Beam Loss Monitors due to their high sensitivity. As discussed earlier, beam losses are at the level of 10^{-5} in LS2. The rms beam emittance is controlled by measuring profiles in multiple locations along the linac [5] to evaluate Courant-Snider parameters and match them to the reference beam envelope defined by the FLAME code.

After one year of operation, the highest residual radiation dose in the tunnel is measured at the BDS with 0.2 mR/hr after 10 days of cool down. This activated spot at the BDS can be related to uncontrolled beam losses. As expected, an elevated residual activation is also measured near the stripper, with 0.14 mR/hr, and near the CSS, with 0.37 mR/hr.

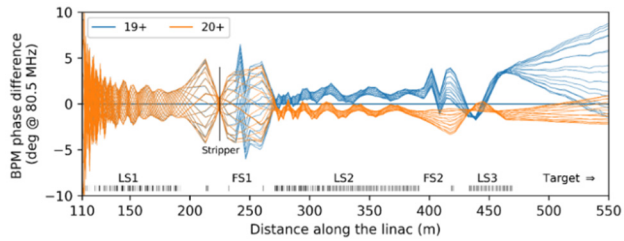

Figure 8: Longitudinal mapping of individual charge states 19+ and 20+ for a ^{48}Ca beam.

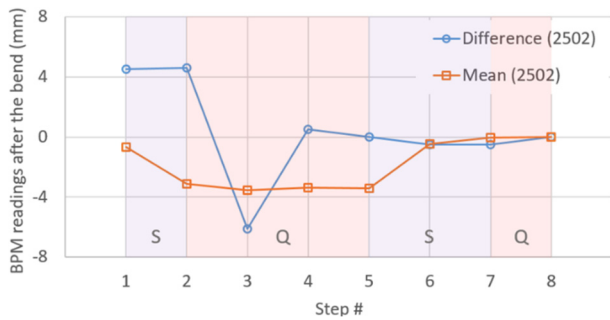

Figure 9: Steps achromatic bend tuning. The shaded areas corresponds to adjustments of sextupoles (purple) and quadrupoles (red).

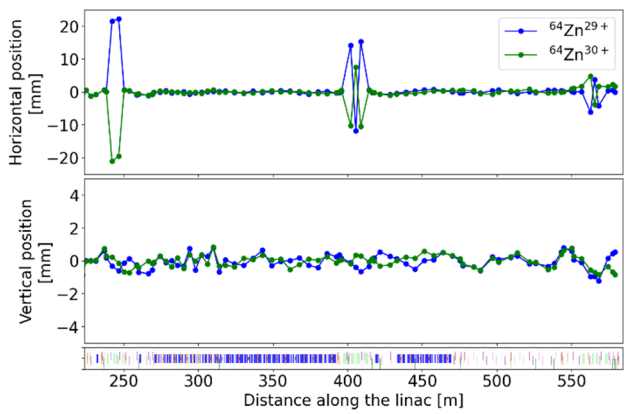

Figure 10: Measured transverse beam position of each charge state of ^{64}Zn beam along the post-stripper linac. Note the scale in the dispersive plane is larger.

DEMONSTRATION OF 10 kW BEAMS

The accelerator operation envelope was extended to 12 kW operation in July. The beam power increase from 5 kW to 10 kW was tested with ^{36}Ar and ^{48}Ca beams and performed as expected. Figure 11 illustrates the

ISBN: 978-3-95450-253-0 ISSN: 2673-5571 doi:10.18429/JACoW-HB2023-MOA1I2

temperature increase on the BDS collimator segments as beam power ramps up to 10 kW. A minor beam steering was applied to equalize the temperatures on the collimator segments. The BLMs readings in the BDS were low and doubled when beam power was increased from 5 to 10 kW. The thermal image of the 10-kW, 217 MeV/u ^{48}Ca beam on the rotating single-slice carbon disk is shown in Fig. 12.

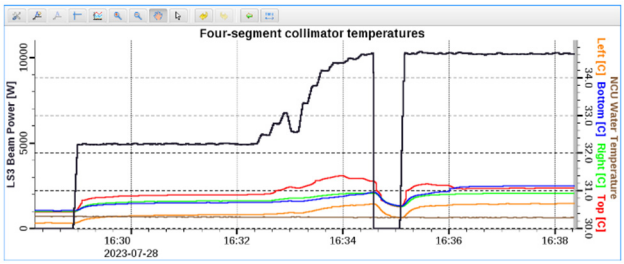

Figure 11: Beam power ramp up from 5 kW to 10 kW on-target and temperatures of 4-segment collimator located 1.5 m up-stream of the target. The plot shows absolute temperatures, and the temperature on the left segment is lower due to the initial offset.

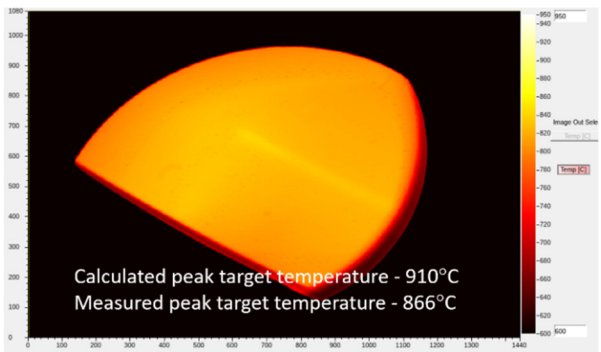

Figure 12: Thermal image of the 10-kW, 217 MeV/u ^{48}Ca beam deposited on the rotating target.

OPERATION

FRIB production runs for the science experiments commenced in May 2022. Once the development of primary and secondary beams is complete, the delivery of isotopes to the experiments has been highly stable. The facility availability is 91%. The leading cause of the downtime was from legacy cryogenic system components and magnets in the secondary beamlines. The Machine Protection System (MPS) operated as expected [2]. During the production run, some adjustments of the ECR were required, especially for metal beams, to maintain constant beam power on-target. The SRF cavities are operated at slightly lower fields than the design to facilitate stable operation and provide a margin for quick recovery in the case of possible failure of some cavities.

POWER RAMP-UP

Based on success in stably delivering a 10 kW beam to the target, the existing linac tunes can be extended to significantly higher power when we upgrade the beam dump and establish the operational safety envelope. At higher power, we expect larger emittances and enhanced beam halo for the beams emerging from the ECRs. This may require additional collimation in the FE. Due to the high sensitivity of SRF cavities to beam losses, we need to keep losses in the LS2 below several watts. There are several R&D projects directly related to beam physics issues in preparation for power ramp-up:

- Activate the energy feedback to minimize beam energy jitter due to sudden changes in the liquid lithium film thickness.
- Develop a second harmonic cavity to linearize the rebuncher voltage downstream of the stripper.
- Develop larger aperture, stronger focusing quadrupoles for use near the stripper to reduce the beam diameter on the stripper to minimize the effect of film non-uniformity.
- Investigate beam losses in the BDS for larger emittance, multiple-charge-state beams. Larger aperture quadrupoles in the BDS may be necessary to avoid beam losses.

The beam power ramp-up also requires significant improvements on the target and beam dump. The existing beam dump limits possible experiments to about 20 kW. Another paper at this workshop [14] comprehensively reviews the accelerator improvement projects geared toward high beam power operation.

SUMMARY

In addition to three-charge-state ion beams, a dual charge state Zn beam was developed and used for science experiments. The linac tune for the acceleration of dual charge state ^{48}Ca beam with the most challenging charge spread of 5% has been demonstrated. The beam power of the linac has been increased 10-fold within 1.5 years. There are presently about 50 approved experiments requesting 10 kW primary beams that can be delivered with high reliability. Higher power, 20 kW ion beams will be available next FY. FRIB is on track to deliver 4400 scheduled hours for the scientific program supporting nuclear physics, and will offer an additional 2000 hours annually for users from industry and single event experiments.

ACKNOWLEDGEMENTS

The authors are grateful to the entire FRIB team for supporting the beam commissioning and operating the machine. The authors thank Prof. S. Lund for carefully reading the manuscript and valuable comments.

REFERENCES

[1] J. Wei *et al.*, "Accelerator commissioning and rare isotope identification at the Facility for Rare Isotope Beams", *Mod. Phys. Lett. A*, vol. 37, no. 9, p. 2230006, 2022. doi:10.1142/S0217732322300063

[2] J. Wei *et al.*, "FRIB Transition to User Operations, Power Ramp up, and Upgrade Perspectives", presented at SRF'23, Grand Rapids, MI, USA, Jun. 2023, paper MOIAA01.

ISBN: 978-3-95450-253-0 ISSN: 2673-5571 doi:10.18429/JACoW-HB2023-MOA1I2

[3] P.N. Ostroumov *et al*., "Status of FRIB Commissioning", in *Proc. HB'21,* Batavia, IL, USA, Oct. 2021, pp. 205-207. doi:10.18429/JACoW-HB2021-WEDC3

[4] P.N. Ostroumov *et al.*, "FRIB Commissioning", in *Proc. HIAT'22*, Darmstadt, Germany, Jun.-Jul. 2022, pp. 118-123. doi:10.18429/JACoW-HIAT2022-WE1I3

[5] P.N. Ostroumov *et al.,* "Accelerator and beam physics challenges in support of FRIB experiments", in *Proc. IPAC'23*, Venice, Italy, May 2023, pp.1729-1732. doi:10.18429/JACoW-IPAC2023-TUPA180

[6] G. Machicoane, D. Cole, J. Ottarson, J. Stetson, and P. Zavodszky, "ARTEMIS-B: A room-temperature test electron cyclotron resonance ion source for the national superconducting cyclotron laboratory at Michigan State University", *Rev. Sci. Instrum.*, vol. 77, p. 03A322, 2006. doi:10.1063/1.2165749

[7] H. Ren *et al.,* "Development and status of the FRIB 28 GHz SC ECRIS", *J. Phys.: Conf. Ser.*, vol. 2244, p. 012008, 2022. doi:10.1088/1742-6596/2244/1/012008

[8] T. Kanemura *et al.,* "Operational Performance with FRIB Liquid Lithium and Carbon Charge Strippers these proceedings", presented at HB'23, Geneva, Switzerland, Oct. 2023, paper WEC2I2, these proceedings.

[9] Experimental Physics and Industrial Control System, https://epics-controls.org/.

[10] T. Zhang, K. Fukushima, M. Ikegami, D. G. Maxwell, and P. N. Ostroumov, "High-level Physics Controls Applications Development for FRIB", in *Proc. ICALEPCS'19*, New York, NY, USA, Oct. 2019, pp.828-834. doi:10.18429/JACoW-ICALEPCS2019-TUCPR07

[11] T. Zhang, K. Fukushima, T. Maruta, P. N. Ostroumov, A. S. Plastun, and Q. Zhao, "Manage the Physics Settings on the Modern Accelerator", in *Proc. ICALEPCS'21*, Shanghai, China, Oct. 2021, pp. 569-573. doi:10.18429/JACoW-ICALEPCS2021-WEBL04

[12] A. S. Plastun and P. N. Ostroumov, "Instant Phase Setting in a Large Superconducting Linac", in *Proc. NAPAC'22*, Albuquerque, NM, USA, Aug. 2022, pp. 885-890. doi:10.18429/JACoW-NAPAC2022-THZD1

[13] Z. He, Y. Zhang, J. Wei, Z. Liu, and R. M. Talman, "Linear envelope model for multi-charge state linac", *Phys. Rev. Accel. Beams*, vol. 17, p. 034001, 2014. doi:10.1103/PhysRevSTAB.17.034001

[14] J. Wei *et al.,* "FRIB Plans Towards High Beam Power", presented at HB'23, Geneva, Switzerland, Oct. 2023, paper THC1I2, these proceedings.